

Elastic properties of eta carbide (η -Fe₂C) from *ab initio* calculations. Application to cryogenically treated gear steel.

Adrian Oila · Chi Lung · Steve Bull

Abstract The elastic properties of η -Fe₂C (eta carbide) have been determined from *ab initio* density functional theory (DFT) calculations using the generalized gradient approximation (GGA). The isotropic polycrystalline elastic modulus of η -Fe₂C has been calculated as the average of anisotropic single-crystal elastic constants determined from the *ab initio* simulations. The calculated polycrystalline elastic modulus was used to compute the elastic modulus of a case carburised gear steel subjected to shallow cryogenic treatment (SCT) and deep cryogenic treatment (DCT). This value was then compared with experimental values obtained from nanoindentation. The results confirmed that the changes in elastic modulus observed in the DCT steel can be attributed to the precipitation of η -Fe₂C. No changes in

hardness have been observed between the SCT steel and the DCT steel. These data were then used to assess the surface contact fatigue behaviour of the SCT and DCT steels tested under elastohydrodynamic lubrication (EHL) conditions.

Keywords Ab initio · Eta carbide · Cryogenic · Contact fatigue

PACS 31.15.A · 61.50.Ah · 61.66.Fn · 81.40.Pq · 81.40.Ef

Introduction

η -Fe₂C (eta carbide) and ϵ -Fe_{2.4}C (epsilon carbide) are two transition compounds which occur in the microstructure of quenched steels during the initial stages of tempering [1]. The precipitation of ϵ -Fe_{2.4}C is predominant in conventional heat treatments (quenching in oil at temperatures above 273 K) while η -Fe₂C precipitates during cryogenic (sub-zero) treatments, known as *shallow* when the quenching temperature is near 193 K and *deep* when the quenching is performed at or near 77 K [2, 3].

A. Oila

School of Chemical Engineering and Advanced Materials

Newcastle University, Newcastle upon Tyne, NE1 7RU

United Kingdom

E-mail: Adrian.Oila@newcastle.ac.uk

The application of cryogenic treatments to steel components such as tools [4–8] and gears [2, 3, 9–18] is justified by numerous claims that the wear and fatigue behaviour is significantly improved mainly due to three phenomena which occur at low temperatures [10]: complete martensitic transformation, changes in the residual stresses and precipitation of nanometric carbides.

The microstructure of surface hardened steels commonly used to manufacture heavy-duty gears typically consists of tempered martensite, retained austenite and iron carbides. The complexity of this microstructure has led to somewhat contradictory opinions regarding the role played by individual phases in wear and contact fatigue. An example for this is the influence of retained austenite and its optimum amount (a brief review can be found in [19]).

A better understanding of the role played by individual phases is necessary for reliable failure predictions and this requires that the mechanical properties of the phases involved are known. Experimental determination of these properties (i.e. elastic modulus, hardness, yield strength, etc.) can be difficult, on one hand because of the small size of the grains (the η -Fe₂C observed [20] varies from 5 to 10 nm in cross-section and from 20 to 40 nm in length) and, on the other hand because some phases are not stable at room temperature (i.e., unalloyed Fe-C austenite). The structure of Fe-C austenite as well as a number of relevant properties have been computed by molecular dynamics [21] but, to

date no experimental or theoretical data exists for the elastic modulus of η -Fe₂C.

The lattice parameter of η -Fe₂C has been determined from *ab initio* calculations by various authors [22–25], its bulk modulus has also been calculated [24, 25] but the anisotropic single-crystal elastic constants have been computed only by Lv *et al.* [25].

Although, the mechanisms by which cryogenic treatments improve the wear resistance of steels are not completely understood it is believed [20] that the precipitation of nanometric η -Fe₂C enhances the strength and toughness of the martensite matrix, similar to the reinforcement of composites with nanoparticles. Also, the precipitation of the nanometric carbides is accompanied by a reduction in residual stresses in martensite [17]. The proposed mechanism [20] of η -Fe₂C formation at low temperatures involves a slight shift of carbon atoms from the equilibrium position due to lattice deformation.

In this work, we determined the structural and elastic properties of η -Fe₂C from first principles. These include the lattice parameters and the single-crystal elastic constants. The isotropic polycrystalline elastic moduli have been calculated as averages of single-crystal elastic constants using the Hill's average [26].

The calculated elastic modulus for η -Fe₂C and the experimentally determined elastic modulus of martensite were used to estimate the elastic modulus of a gear steel subjected

to two different cryogenic treatments: shallow (SCT) and deep (DCT), respectively by applying the rule of mixtures (Eq. 13). These data were then used to assess the contact fatigue behaviour of the steel tested under rolling/sliding elastohydrodynamic lubrication (EHL) conditions.

At the time of writing there is no published work on the wear behaviour of cryogenically treated gear steels under EHL conditions (in which most case carburised gears operate).

Ab initio calculations

The crystal structure of η -Fe₂C (Fig. 1) is orthorhombic [1, 27–29], space group *Pnnm* (58), with 6 atoms in the conventional unit cell: 4 Fe atoms and 2 C atoms. The Wyckoff positions of the atoms are Fe 4g ($x, 0.25, 0$) and C 2a ($0, 0, 0$). The experimentally measured lattice parameters [27] $a = 4.704$ Å, $b = 4.318$ Å and $c = 2.830$ Å were used as initial values in the simulations. The *ab initio* spin-polarized calculations were performed employing the generalized gradient approximation (GGA) [30] as implemented in the Quantum-ESPRESSO package [31], using atomic ultrasoft pseudopotentials [32] within the density functional theory (DFT) [33, 34]. The use of generalized gradient approximation (GGA) is preferred because it correctly predicts the ferromagnetic body centred cubic (BCC) structure of Fe, while the local density approximation (LDA) incorrectly predicts its ground state to be nonmagnetic [35].

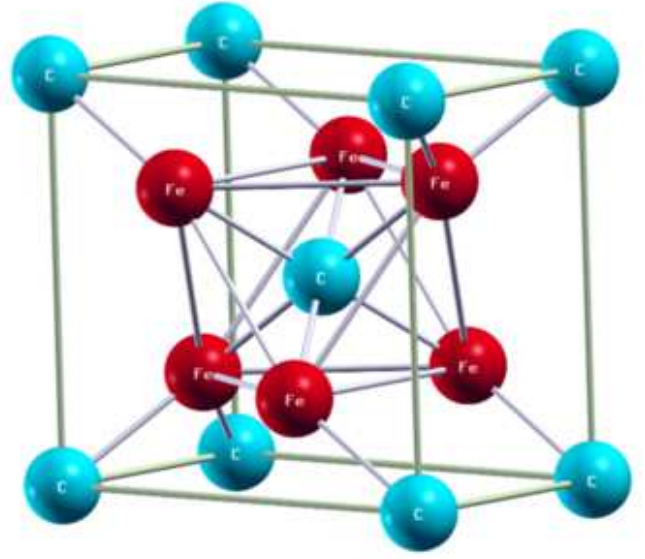


Fig. 1 The orthorhombic unit cell of η -Fe₂C.

The Brillouin zone was sampled by constructing a k -points mesh following the Monkhorst-Pack scheme [36] in which the k -points are homogeneously distributed in rows and columns running parallel to the reciprocal vectors. The Brillouin zone integrations were performed using a Marzari-Vanderbilt method [37] with a Gaussian spreading of 0.005 Ry (~ 0.068 eV). A mesh $6 \times 7 \times 10$ which gives 264 k -points in the Brillouin zone was selected for consequent calculations. Fig. 2 shows the energy values computed for different k -points meshes. For meshes containing 264 or more k -points all energy values lie within a window of 1 meV.

After the convergence tests, a plane wave kinetic-energy cutoff of 65 Ry (~ 884 eV) and a charge density cutoff of 390 Ry (~ 5306 eV) were found to be sufficient to converge the total energy to less than 5 meV/atom (Fig. 3).

Structural optimisation was performed by computing the total energy as a function of the unit cell volume by varying the b/a and c/a ratios while allowing the atomic coordinates to relax according to a conjugate-gradient scheme. The calculated energy was plotted versus the unit cell volume (Fig. 4) and fitted to the Murnaghan equation of state [38].

The elastic constants, c_{ij} , of the orthorhombic unit cell were calculated by applying a small strain to the equilibrium lattice parameter and computing the total energy. The symmetric distortion matrix for an orthorhombic unit cell, \mathbf{D} , is given by [35]:

$$\mathbf{D} = \begin{pmatrix} 1 + \varepsilon_1 & \varepsilon_6/2 & \varepsilon_5/2 \\ \varepsilon_6/2 & 1 + \varepsilon_2 & \varepsilon_4/2 \\ \varepsilon_5/2 & \varepsilon_4/2 & 1 + \varepsilon_3 \end{pmatrix} \quad (1)$$

where ε_i are the strain tensor components in Voigt notation. The elastic constants, c_{ij} , can be calculated from the Hook's law. Fig. 5 shows an example of linear fitting of the calculated stress versus the applied strain. The corresponding elastic constant represents the slope of the fitted curve.

The polycrystalline bulk modulus B (Eq. 2) and shear modulus G (Eq. 3) can be calculated using the Hill's average [26]:

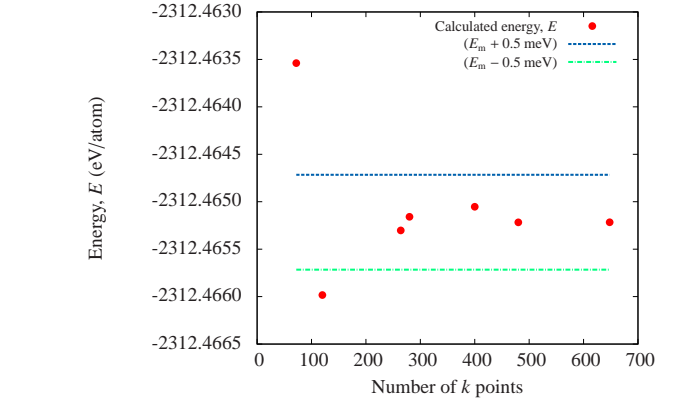


Fig. 2 Energy function of the number of k -points in the Brillouin zone.

E_m = the energy computed using the most dense mesh.

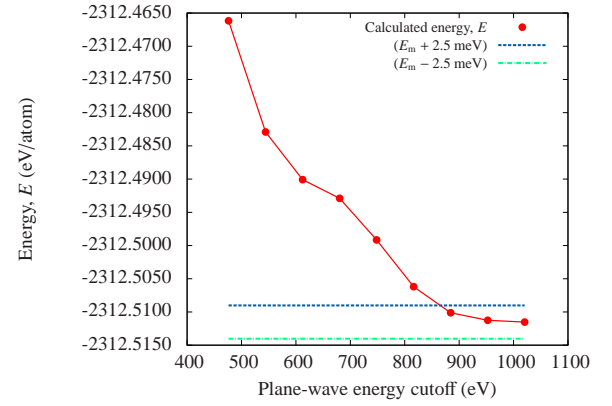


Fig. 3 Energy convergence test for η -Fe₂C. E_m = the energy computed using the highest energy cutoff.

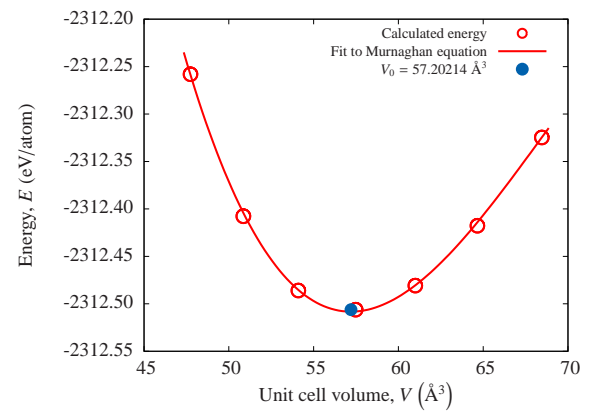


Fig. 4 Calculated energy as a function of the η -Fe₂C unit cell volume.

$$B = \frac{B_{\text{Reuss}} + B_{\text{Voigt}}}{2} \quad (2)$$

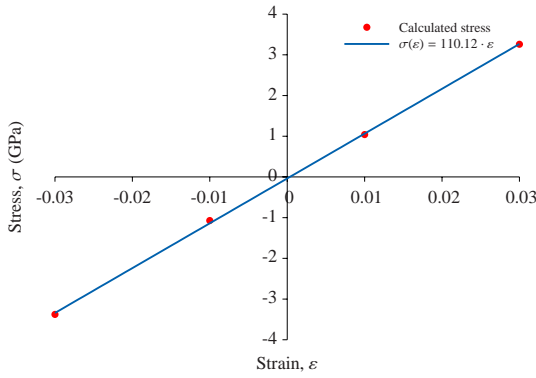


Fig. 5 Calculation of elastic constant $c_{44} = 110.12$ GPa.

$$G = \frac{G_{Reuss} + G_{Voigt}}{2} \quad (3)$$

where B_{Reuss} and G_{Reuss} are given by Eq. 4 and 5 assuming uniform stress [39] and B_{Voigt} and G_{Voigt} are given by Eq. 6 and 7 assuming uniform strain [40].

$$B_{Reuss} = \frac{1}{s_{11} + s_{22} + s_{33} + 2(s_{12} + s_{23} + s_{13})} \quad (4)$$

$$G_{Reuss} = \frac{15}{4(s_{11} + s_{22} + s_{33} - s_{12} - s_{23} - s_{13}) + 3(s_{44} + s_{55} + s_{66})} \quad (5)$$

$$B_{Voigt} = \frac{c_{11} + c_{22} + c_{33} + 2(c_{12} + c_{23} + c_{13})}{9} \quad (6)$$

$$G_{Voigt} = \frac{c_{11} + c_{22} + c_{33} - c_{12} - c_{23} - c_{13}}{15} + \frac{c_{44} + c_{55} + c_{66}}{5} \quad (7)$$

The elastic modulus, E , and the Poisson's ratio, ν , can be calculated using Eq. 8 and 9, respectively.

$$E = \frac{9BG}{3B + G} \quad (8)$$

$$\nu = \frac{3B/2 - G}{3B + G} \quad (9)$$

Experimental

Tests were carried out on samples of S156 steel which had been carburised, quenched and surface ground. The chemical composition of the S156 steel is given in Table 1. The cryogenic treatments (SCT and DCT) were carried out at Frozen Solid UK after tempering at 190°C. The depth of the hardened case after grinding was approximately 1 mm. The surface finish measured by optical profilometry was $R_a = 0.2 - 0.4 \mu\text{m}$, a value similar to that commonly obtained in gears. The retained austenite content has been measured by X-Ray diffraction using a XSTRESS 3000 (Stresstech Group) stress analyser. The values corresponding to the depth below surface at which the nanoindentation tests were carried out (500 μm) are given in Table 5.

Nanoindentation

The nanoindentation tests were carried out using a Hysitron Triboindenter with a Berkovich tip using a maximum applied load of 10 mN. After each indentation an area $5 \times 5 \mu\text{m}$ was scanned using the AFM (Atomic Force Microscope) of

Table 1 Chemical composition of S156 steel, wt %.

C	Si	Mn	P	S	Cr	Mo	Ni
0.14-0.18	0.10-0.35	0.25-0.55	max. 0.015	max. 0.012	1.00-1.40	0.20-0.30	3.80-4.30

the triboindenter. Hardness, H (Eq. 10) and elastic modulus, E (Eq. 11 and 12) have been calculated using the Oliver-Pharr method [41].

$$H = \frac{P_{max}}{A_c} \quad (10)$$

where:

P_{max} is the maximum indentation load

A_c is the projected area of tip-sample contact

$$E^* = \frac{1}{2} \sqrt{\frac{\pi}{A_c}} S \quad (11)$$

where:

E^* is the reduced contact modulus

S is the stiffness

$$\frac{1}{E^*} = \frac{1 - \nu^2}{E} + \frac{1 - \nu_i^2}{E_i} \quad (12)$$

where:

ν and ν_i are the Poisson's ratios of sample and indenter, respectively

E and E_i are the Young's moduli of sample and indenter, respectively

A total of 50 indentations have been performed on a polished cross section of each sample at a depth of approximately 500 μm .

Surface contact fatigue

The surface contact fatigue tests have been carried out using a rig described in a previous publication [42]. A number of six pairs of discs have been tested: two oil quenched, two shallow cryogenic treated and two deep cryogenic treated. In the conventional treatment the samples were oil quenched from 825 °C, and tempered at 190 °C.

In order to achieve an elliptical contact, one of the discs was crowned with a crown height of 5 mm, giving a crown radius of 250 mm. All contact fatigue tests have been carried out for 5×10^5 cycles under a contact pressure 1.5 GPa, at a temperature of 60 °C and a speed of 1200 rev/min with a slide-to-roll ratio of 0.33. The lubricant used was Valvoline HP Gear Oil 85W-140 1/5 GA and the calculated λ ratio varied between 0.2 and 0.5.

The type of failure on all specimens, as observed by reflected light microscopy (RLM) and scanning electron microscopy (SEM) was predominantly micropitting (see Fig. 9). The distribution of the micropits inside the contact area,

around the circumference of the disc, follows a uniform pattern which allows for the computation of the average percentage area of damage. The percentage damage has been measured by processing the images captured with a reflected light microscope, and it was determined as the average of 10 measurements taken in different locations chosen at random on the disc surface.

Results and discussion

Calculated properties of η -Fe₂C

The results calculated in this work have been compared with those obtained by others (where available). The calculated lattice parameters are generally in good agreement with values reported by other authors (Table 2).

Table 2 Lattice parameters (Å) of η -Fe₂C.

Source	<i>a</i>	<i>b</i>	<i>c</i>
This study	4.722	4.271	2.835
[28]	4.704	4.318	2.830
[24]	4.687	4.261	2.830
[25]	4.677	4.293	2.814
[23]	4.651	4.258	2.805
[22]	4.708	4.281	2.824

The single-crystal elastic constants of η -Fe₂C are presented in Tabel 3. There are significant differences between the values calculated in the present study and those obtained by Lv *et al.* [25]. The accuracy of the calculated elastic con-

stants is strongly dependant on the accuracy of the self consistency runs and also on the convergence criteria of geometry optimizations for each distorted structure. In our calculations we have used a denser *k*-points mesh ($6 \times 7 \times 10$ compared to $6 \times 6 \times 9$ in [25]) and we imposed a convergence threshold of 10^{-8} Ry ($\sim 1.36 \times 10^{-7}$ eV) while the convergence threshold used in [25] was 10^{-5} eV.

The bulk modulus, *B*, (Tabel 4) calculated in this work agrees well with the values reported by Lv *et al.* [25] and is about 8% different than that reported by Faraoun *et al.* [24]. For shear modulus, *G*, Poisson's ratio, ν , and elastic modulus, *E*, (Tabel 4) no data is available for comparison.

Table 4 Polycrystalline elastic moduli of η -Fe₂C (GPa).

Source	<i>B</i> (GPa)	<i>G</i> (GPa)	<i>E</i> (GPa)	ν
This study	223	147	362	0.23
[24]	243	-	-	-
[25]	226	-	-	-

Nanoindentation

The average elastic modulus of martensite, determined from nanoindentation tests carried out on the oil quenched samples was $E = 203$ GPa and it was used as the reference value in the subsequent calculations of the volume fraction of carbides. The average elastic modulus of retained austenite was $E = 175$ GPa. Similar values were reported for the elastic

Table 3 Elastic constants of η -Fe₂C (GPa).

Source	c_{11}	c_{22}	c_{33}	c_{12}	c_{23}	c_{13}	c_{44}	c_{55}	c_{66}
This study	323	340	378	189	158	136	110	97	136
[25]	310	346	296	170	216	170	64	148	157

Table 5 Retained austenite measurements (%).

Sample	DCT	SCT	Oil quenched
Retained austenite (%)	7.7 ± 0.6	9.3 ± 0.7	23.3 ± 4.1

modulus of Fe-C austenite from molecular dynamics calculations [21].

Considering the percentages of retained austenite determined by XRD (Table 5) and the elastic modulus of each phase which contributes to the measured elastic modulus, the volume fraction of carbides can be estimated using the rule of mixtures (Eq. 13). The phases considered are martensite ($E = 203$ GPa), retained austenite ($E = 175$ GPa) and η -Fe₂C ($E = 362$ GPa). The resulting volume fractions of carbides calculated using the rule of mixtures (Eq. 13) are $f_{DCT} = 0.20$ and $f_{SCT} = 0.04$.

$$E = \sum_{k=1}^n E_k \cdot v_k \quad (13)$$

where:

E is the elastic modulus of composite

E_k is the elastic modulus of phase k

v_k is the volume fraction of phase k

These results show that only a small amount (4%) of η -Fe₂C precipitates during SCT while during DCT a

large number of carbides will form (20%). Typical load-displacement curves obtained for the SCT and DCT steels are shown in Fig. 6. It can be seen that the total displacement at the maximum applied load and the elastic recovery are slightly larger for the SCT steel. The measured hardness and elastic modulus are plotted in Fig. 7(a) and 7(b), respectively. Both, hardness and elastic modulus show little scattering which indicate that the microstructure (see Fig. 8) is relatively homogeneous. The average hardness values are $H_{DCT} = 13.8 \pm 0.6$ GPa for DCT steel and $H_{SCT} = 13.7 \pm 0.6$ GPa for SCT steel. The average elastic modulus was $E_{DCT} = 233.7 \pm 4.4$ GPa for DCT steel and $E_{SCT} = 206.7 \pm 3.7$ GPa for SCT steel.

Surface contact fatigue

Compared to conventional oil quenching, both cryogenic treatments lead to a reduction of micropitting (see Fig. 9).

Table 6 shows the average area of micropitting measured for each specimen.

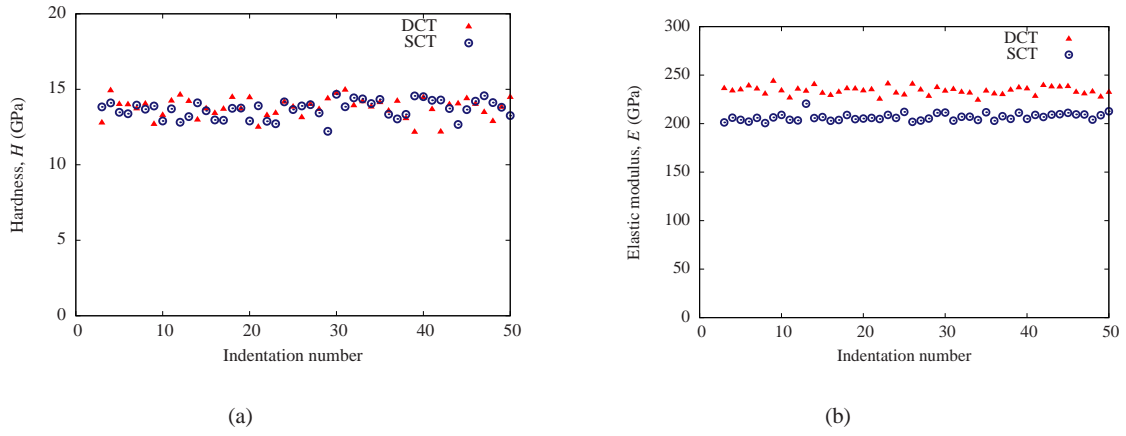


Fig. 7 Nanoindentation results. (a) Hardness; (b) Elastic modulus.

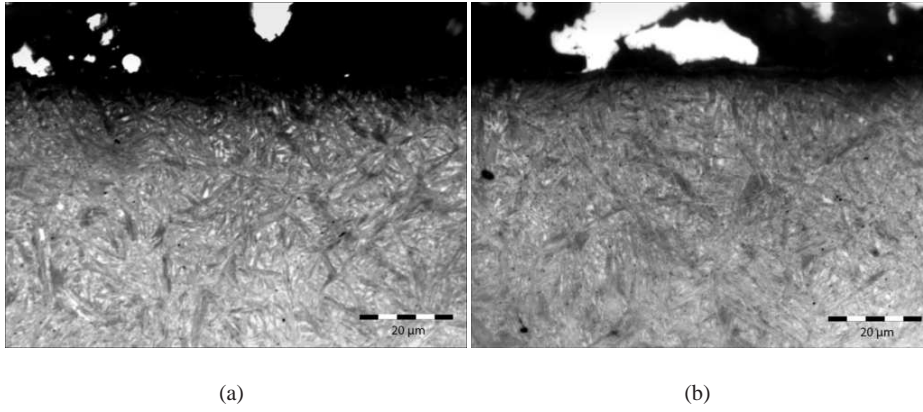


Fig. 8 Microstructure of (a) SCT specimen; (b) DCT specimen. Picral etch.

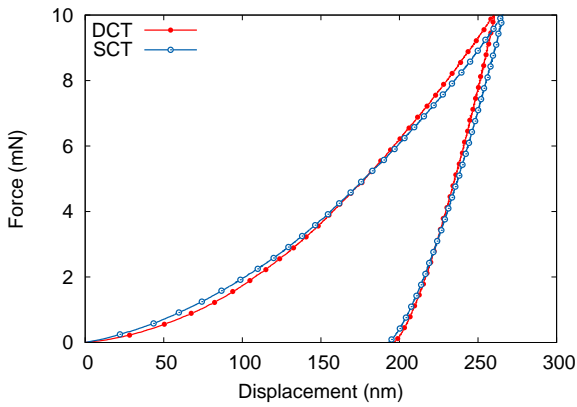


Fig. 6 Load-displacement curves for the two steels.

Both cryogenic treatments are effective in improving the contact fatigue resistance but due to different effects. Since the precipitation of η -Fe₂C in the SCT steel is not signifi-

cant (4%) the improvement is probably due the transformation of retained austenite. On the other hand, the intense precipitation of η -Fe₂C in the DCT steel (20%) increases the fracture toughness of martensite by a mechanism specific to metal matrix composites: (1) crack deflection by the stiffer nanoparticle, (2) crack trapping by nanoparticle which results in significant reduction of stresses in the matrix and, (3) crack bridging ahead of the main crack tip.

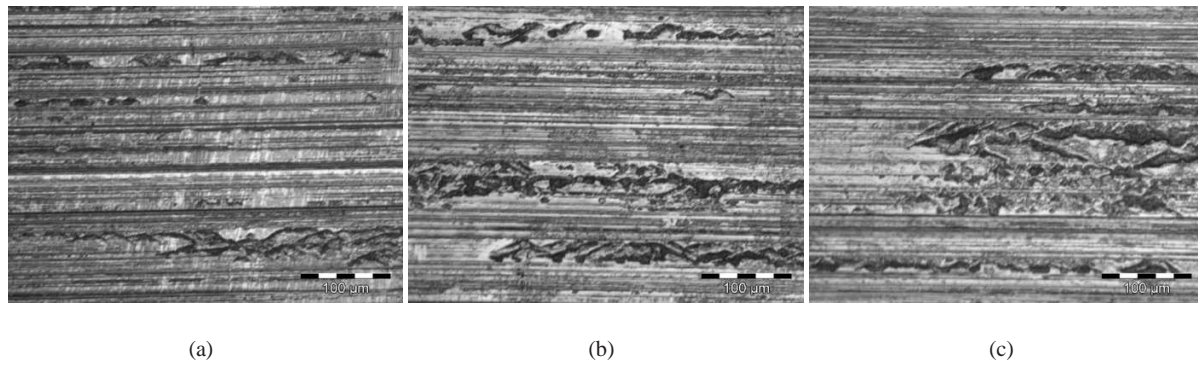


Fig. 9 Light microscopy images showing the surface of (a) DCT sample; (b) SCT sample; (c) oil quenched sample.

Table 6 Average micropitting area, M (%).

Sample	DCT	SCT	Oil quenched
M (%)	4.2 ± 1.2	5.8 ± 1.4	8.2 ± 1.5

Conclusions

In this work the elastic properties of η -Fe₂C have been determined from *ab initio* calculations. The hardness and elastic modulus of a case carburised gear steel subjected to cryogenic treatments (SCT and DCT) have been determined by nanoindentation. Based on the elastic modulus of η -Fe₂C derived from first principles the volume fraction of carbides was estimated. It was found that the microstructure of the SCT steel contains only 4% of η -Fe₂C the microstructure of the DCT steel contains 20% of η -Fe₂C. The precipitation of eta carbide in the DCT steel results in an increase in elastic modulus but there is no difference in the hardness of the DCT steel and SCT steel.

The micropitting tests carried out under EHL conditions showed that cryogenic treatments improved the surface con-

tact fatigue behaviour of S156 case carburised steel. The average micropitting area was 8.2% for the oil quenched steel, 5.8% for the SCT steel and 4.2% for the DCT steel. Both cryogenic treatments are effective in reducing micropitting but the mechanisms involved are probably different. The improved contact fatigue performance of the SCT steel is due to the transformation of retained austenite while in the DCT steel this is due to an increase in fracture toughness as a result of eta carbide precipitation. The nano-carbides act as reinforcements in the martensite matrix by one of the mechanisms specific to composite materials: (1) crack deflection, (2) crack trapping and, (3) crack bridging.

Acknowledgements The authors thank Frozen Solid for carrying out the cryogenic treatments. Special thanks to Chris Aylott from the Design Unit - Newcastle University for fruitful discussions and for carrying out the retained austenite measurements.

References

1. Y. Nakamura, S. Nagakura, Transactions of the Japan Institute of Metals **27**(11), 842 (1986)
2. P. Baldissera, C. Delprete, The Open Mechanical Engineering Journal (2), 1 (2008)
3. A. Bensely, A. Prabhakaran, D. Mohan Lal, G. Nagarajan, Cryogenics **45**(12), 747 (2006). DOI 10.1016/j.cryogenics.2005.10.004
4. D. Das, A. Dutta, K. Ray, Wear **267**(9-10), 1371 (2009). DOI 10.1016/j.wear.2008.12.051
5. D. Das, A.K. Dutta, K.K. Ray, Materials Science and Engineering A **527**(9), 2182 (2010). DOI 10.1016/j.msea.2009.10.070
6. D. Das, A.K. Dutta, K.K. Ray, Materials Science and Engineering A **527**(9), 2194 (2010). DOI 10.1016/j.msea.2009.10.071
7. V. Firouzdor, E. Nejati, F. Khomamizadeh, Journal of Materials Processing Technology **206**(1-3), 467 (2008). DOI 10.1016/j.jmatprotec.2007.12.072
8. A. Molinari, M. Pellizzari, S. Gialanella, G. Straffelini, K. Stiasny, (2001), vol. 118, pp. 350–355. DOI 10.1016/S0924-0136(01)00973-6
9. P. Baldissera, Materials and Design **30**(9), 3636 (2009). DOI 10.1016/j.matdes.2009.02.019
10. P. Baldissera, C. Delprete, Materials and Design **30**(5), 1435 (2009). DOI 10.1016/j.matdes.2008.08.015
11. A. Bensely, D. Senthilkumar, D. Mohan Lal, G. Nagarajan, A. Rajadurai, Materials Characterization **58**(5), 485 (2007). DOI 10.1016/j.matchar.2006.06.019
12. A. Bensely, S. Venkatesh, D. Mohan Lal, G. Nagarajan, A. Rajadurai, K. Junik, Materials Science and Engineering A **479**(1-2), 229 (2008). DOI 10.1016/j.msea.2007.07.035
13. A. Bensely, L. Shyamala, S. Harish, D. Mohan Lal, G. Nagarajan, K. Junik, A. Rajadurai, Materials and Design **30**(8), 2955 (2009). DOI 10.1016/j.matdes.2009.01.003
14. A. Bensely, D. Senthilkumar, S. Harish, D. Mohan Lal, G. Nagarajan, A. Rajadurai, P. Paulin, Gear Solutions pp. 37–51 (2011)
15. V. Manoj, K. Gopinath, G. Muthuveerappan, International Symposium of Research Students on Material Science and Engineering pp. 1–11 (2004)
16. P. Paulin, Gear Technology **10**(2), 26 (1993)
17. M. Preciado, P. Bravo, J. Alegre, Journal of Materials Processing Technology **176**(1-3), 41 (2006). DOI 10.1016/j.jmatprotec.2006.01.011
18. P. Stratton, M. Graf, Cryogenics **49**(7), 346 (2009). DOI 10.1016/j.cryogenics.2009.03.007
19. A. Oila, Micropitting and Related Phenomena in Case Carburised Gears. Ph.D. thesis, Newcastle University (2003)

20. F. Meng, K. Tagashira, R. Azuma, H. Sohma, *ISIJ International* **34**(2), 205 (1994)
21. A. Oila, S. Bull, *Computational Materials Science* **45**(2), 235 (2009). DOI 10.1016/j.commatsci.2008.09.013
22. C.K. Ande, M.H. Sluiter, *Metallurgical and Materials Transactions A* **43A**, 4436 (2012). DOI 10.1007/s11661-012-1229-y
23. L.L. Bao, C.F. Huo, C.M. Deng, Y.W. Li, *Ranliao Huaxue Xuebao/Journal of Fuel Chemistry and Technology* **37**(1), 104 (2009)
24. H. Faraoun, Y. Zhang, C. Esling, H. Aourag, *Journal of Applied Physics* **99**(9), 093508 (2006). DOI 10.1063/1.2194118
25. Z. Lv, S. Sun, P. Jiang, B. Wang, W. Fu, *Computational Materials Science* **42**(4), 692 (2008). DOI 10.1016/j.commatsci.2007.10.007
26. R. Hill, *Physical Society – Proceedings* **65**(389A), 349 (1952)
27. M. Dirand, L. Afqir, *Acta Metallurgica* **31**(7), 1089 (1983). DOI 10.1016/0001-6160(83)90205-5
28. Y. Hirotsu, S. Nagakura, *Acta Metallurgica* **20**(4), 645 (1972)
29. S. Nagakura, Y. Hirotsu, M. Kusunoki, T. Suzuki, Y. Nakamura, *Metallurgical Transactions. A, Physical metallurgy and materials science* **14A**(6), 1025 (1981)
30. J.P. Perdew, K. Burke, M. Ernzerhof, *Phys. Rev. Lett.* **77**, 3865 (1996). DOI 10.1103/PhysRevLett.77.3865
31. P. Giannozzi, S. Baroni, N. Bonini, M. Calandra, R. Car, C. Cavazzoni, D. Ceresoli, G.L. Chiarotti, M. Cococcioni, I. Dabo, A. Dal Corso, S. De Gironcoli, S. Fabris, G. Fratesi, R. Gebauer, U. Gerstmann, C. Gougoussis, A. Kokalj, M. Lazzeri, L. Martin-Samos, N. Marzari, F. Mauri, R. Mazzarello, S. Paolini, A. Pasquarello, L. Paulatto, C. Sbraccia, S. Scandolo, G. Sclauzero, A.P. Seitsonen, A. Smogunov, P. Umari, R.M. Wentzcovitch, *Journal of Physics Condensed Matter* **21**(39), 395502 (2009). DOI 10.1088/0953-8984/21/39/395502
32. K. Laasonen, A. Pasquarello, R. Car, C. Lee, D. Vanderbilt, *Phys. Rev. B* **47**, 10142 (1993). DOI 10.1103/PhysRevB.47.10142
33. P. Hohenberg, W. Kohn, *Phys. Rev.* **136**, B864 (1964). DOI 10.1103/PhysRev.136.B864
34. W. Kohn, L.J. Sham, *Phys. Rev.* **140**, A1133 (1965). DOI 10.1103/PhysRev.140.A1133
35. C. Jiang, S. Srinivasan, A. Caro, S. Maloy, *Journal of Applied Physics* **103**(4), 043502 (2008). DOI 10.1063/1.2884529
36. H.J. Monkhorst, J.D. Pack, *Phys. Rev. B* **13**, 5188 (1976). DOI 10.1103/PhysRevB.13.5188
37. N. Marzari, D. Vanderbilt, A. De Vita, M.C. Payne, *Phys. Rev. Lett.* **82**, 3296 (1999). DOI 10.1103/PhysRevLett.82.3296

-
38. F. Murnaghan, Proc Natl Acad Sci U. S. A. **30**(9), 244
(1944)
 39. A. Reuss, Zeitschrift für Angewandte Mathematik und
Mechanik **9**(1), 49 (1929)
 40. W. Voigt, Königliche Gesellschaft der Wissenschaften
zu Göttingen **34**(3–100) (1887)
 41. W. Oliver, G. Pharr, Journal of Materials Research **7**(6),
1564 (1992)
 42. A. Oila, S. Bull, Wear **258**(10), 1510 (2005). DOI 10.
1016/j.wear.2004.10.012